CERN-PH-EP-2014-096
May 16, 2014

Spin alignment and violation of the OZI rule in exclusive ω and ϕ production in pp collisions

The COMPASS Collaboration

Abstract

Exclusive production of the isoscalar vector mesons ω and ϕ is measured with a 190 GeV/c proton beam impinging on a liquid hydrogen target. Cross section ratios are determined in three intervals of the Feynman variable x_F of the fast proton. A significant violation of the OZI rule is found, confirming earlier findings. Its kinematic dependence on x_F and on the invariant mass M_{pV} of the system formed by fast proton p_{fast} and vector meson V is discussed in terms of diffractive production of $p_{\text{fast}}V$ resonances in competition with central production. The measurement of the spin density matrix element ρ_{00} of the vector mesons in different selected reference frames provides another handle to distinguish the contributions of these two major reaction types. Again, dependences of the alignment on x_F and on M_{pV} are found. Most of the observations can be traced back to the existence of several excited baryon states contributing to ω production which are absent in the case of the ϕ meson. Removing the low-mass M_{pV} resonant region, the OZI rule is found to be violated by a factor of eight, independently of x_F .

PACS: 13.30.Eg, 13.85Hd, 13.88.+e, 14.40Be

Keywords: OZI rule, vector meson production, tensor polarisation, experimental results

(to be submitted to Nucl. Phys. B)

The COMPASS Collaboration

C. Adolph⁸, R. Akhunzyanov⁷, M.G. Alexeev²⁷, G.D. Alexeev⁷, A. Amoroso^{27,29}, V. Andrieux²², V. Anosov⁷, A. Austregesilo^{10,17}, B. Badełek³¹, F. Balestra^{27,29}, J. Barth⁴, G. Baum¹, R. Beck³, Y. Bedfer²², A. Berlin², J. Bernhard¹³, K. Bicker^{10,17}, J. Bieling⁴, R. Birsa²⁵, J. Bisplinghoff³, M. Bodlak¹⁹, M. Boer²², P. Bordalo^{12,a}, F. Bradamante^{24,25}, C. Braun⁸, A. Bressan^{24,25}, M. Büchele⁹, E. Burtin²², L. Capozza²², M. Chiosso^{27,29}, S.U. Chung^{17,b}, A. Cicuttin^{26,25}, M.L. Crespo^{26,25}, Q. Curiel²², S. Dalla Torre²⁵, S.S. Dasgupta⁶, S. Dasgupta²⁵, O.Yu. Denisov²⁹, S.V. Donskov²¹, N. Doshita³³, V. Duic²⁴, W. Dünneberger¹⁶, M. Dziewiecki³², A. Efremov⁷, C. Elia^{24,25}, P.D. Eversheim³, W. Eyrich⁸, M. Faessler¹⁶, A. Ferrero²², A. Filin²¹, M. Finger¹⁹, M. Finger jr.¹⁹, H. Fischer⁹, C. Franco¹², N. du Fresne von Hohenesche^{13,10}, J.M. Friedrich¹⁷, V. Frolov¹⁰, F. Gautheron², O.P. Gavrichtchouk⁷, S. Gerassimov^{15,17}, R. Geyer¹⁶, I. Gnesi^{27,29}, B. Gobbo²⁵, S. Goertz⁴, M. Gorzelli⁹, S. Grabmüller¹⁷, A. Grasso^{27,29}, B. Grube¹⁷, T. Grussenmeyer⁹, A. Guskov⁷, T. Guthörl^{9,c}, F. Haas¹⁷, D. von Harrach¹³, D. Hahne⁴, R. Hashimoto³³, F.H. Heinsius⁹, F. Herrmann⁹, F. Hinterberger³, Ch. Höppner¹⁷, N. Horikawa^{18,d}, N. d'Hose²², S. Huber¹⁷, S. Ishimoto^{33,e}, A. Ivanov⁷, Yu. Ivanshin⁷, T. Iwata³³, R. Jahn³, V. Jary²⁰, P. Jasinski¹³, P. Jörg⁹, R. Joosten³, E. Kabuß¹³, B. Ketzer^{17,f}, G.V. Khaustov²¹, Yu.A. Khokhlov^{21,g}, Yu. Kisselev⁷, F. Klein⁴, K. Klimaszewski³⁰, J.H. Koivuniemi², V.N. Kolosov²¹, K. Kondo³³, K. Königsman⁹, I. Konorov^{15,17}, V.F. Konstantinov²¹, A.M. Kotzinian^{27,29}, O. Kouznetsov⁷, M. Krämer¹⁷, Z.V. Kroumchtein⁷, N. Kuchinski⁷, F. Kunne²², K. Kurek³⁰, R.P. Kurjata³², A.A. Lednev²¹, A. Lehmann⁸, M. Levillain²², S. Levorato²⁵, J. Lichtenstadt²³, A. Maggiora²⁹, A. Magnon²², N. Makke^{24,25}, G.K. Mallot¹⁰, C. Marchand²², A. Martin^{24,25}, J. Marzec³², J. Matousek¹⁹, H. Matsuda³³, T. Matsuda¹⁴, G. Meshcheryakov⁷, W. Meyer², T. Michigami³³, Yu.V. Mikhailov²¹, Y. Miyachi³³, A. Nagaytsev⁷, T. Nagel¹⁷, F. Nerling¹³, S. Neubert¹⁷, D. Neyret²², V.I. Nikolaenko²¹, J. Novy²⁰, W.-D. Nowak⁹, A.S. Nunes¹², A.G. Olshevsky⁷, I. Orlov⁷, M. Ostrick¹³, R. Panknin⁴, D. Panzieri^{28,29}, B. Parsamyan^{27,29}, S. Paul¹⁷, S. Platchkov²², J. Pochodzalla¹³, V.A. Polyakov²¹, J. Pretz^{4,h}, M. Quaresma¹², C. Quintans¹², S. Ramos^{12,a}, C. Regali⁹, G. Reicherz², E. Rocco¹⁰, N.S. Rossiyskaya⁷, D.I. Ryabchikov²¹, A. Rychter³², V.D. Samoylenko²¹, A. Sandacz³⁰, M. Sapozhnikov⁷, S. Sarkar⁶, I.A. Savin⁷, G. Sbrizzai^{24,25}, P. Schiavon^{24,25}, C. Schill⁹, T. Schlüter¹⁶, K. Schmidt^{9,c}, H. Schmieden⁴, K. Schönning¹⁰, S. Schopferer⁹, M. Schott¹⁰, O.Yu. Shevchenko^{7,*}, L. Silva¹², L. Sinha⁶, S. Sirtl⁹, M. Slunicka⁷, S. Sosio^{27,29}, F. Sozzi²⁵, A. Srnka⁵, L. Steiger²⁵, M. Stolarski¹², M. Sulc¹¹, R. Sulej³⁰, H. Suzuki^{33,d}, A. Szabelski³⁰, T. Szameitat^{9,c}, P. Sznajder³⁰, S. Takekawa^{27,29}, J. ter Wolbeek^{9,c}, S. Tessaro²⁵, F. Tessarotto²⁵, F. Thibaud²², S. Uhl¹⁷, I. Uman¹⁶, M. Virius²⁰, L. Wang², T. Weisrock¹³, M. Wilfert¹³, R. Windmolders⁴, H. Wollny²², K. Zaremba³², M. Zavertyaev¹⁵, E. Zemlyanichkina⁷ and M. Ziembicki³², A. Zink⁸

¹ Universität Bielefeld, Fakultät für Physik, 33501 Bielefeld, Germanyⁱ

² Universität Bochum, Institut für Experimentalphysik, 44780 Bochum, Germany^{iP}

³ Universität Bonn, Helmholtz-Institut für Strahlen- und Kernphysik, 53115 Bonn, Germanyⁱ

⁴ Universität Bonn, Physikalisches Institut, 53115 Bonn, Germanyⁱ

⁵ Institute of Scientific Instruments, AS CR, 61264 Brno, Czech Republic^j

⁶ Matrivani Institute of Experimental Research & Education, Calcutta-700 030, India^k

⁷ Joint Institute for Nuclear Research, 141980 Dubna, Moscow region, Russia^l

⁸ Universität Erlangen–Nürnberg, Physikalisches Institut, 91054 Erlangen, Germanyⁱ

⁹ Universität Freiburg, Physikalisches Institut, 79104 Freiburg, Germany^{iP}

¹⁰ CERN, 1211 Geneva 23, Switzerland

¹¹ Technical University in Liberec, 46117 Liberec, Czech Republic^j

¹² LIP, 1000-149 Lisbon, Portugal^m

¹³ Universität Mainz, Institut für Kernphysik, 55099 Mainz, Germanyⁱ

¹⁴ University of Miyazaki, Miyazaki 889-2192, Japanⁿ

- ¹⁵ Lebedev Physical Institute, 119991 Moscow, Russia
- ¹⁶ Ludwig-Maximilians-Universität München, Department für Physik, 80799 Munich, Germany^{io}
- ¹⁷ Technische Universität München, Physik Department, 85748 Garching, Germany^{io}
- ¹⁸ Nagoya University, 464 Nagoya, Japanⁿ
- ¹⁹ Charles University in Prague, Faculty of Mathematics and Physics, 18000 Prague, Czech Republic^j
- ²⁰ Czech Technical University in Prague, 16636 Prague, Czech Republic^j
- ²¹ State Scientific Center Institute for High Energy Physics of National Research Center ‘Kurchatov Institute’, 142281 Protvino, Russia
- ²² CEA IRFU/SPhN Saclay, 91191 Gif-sur-Yvette, France^p
- ²³ Tel Aviv University, School of Physics and Astronomy, 69978 Tel Aviv, Israel^q
- ²⁴ University of Trieste, Department of Physics, 34127 Trieste, Italy
- ²⁵ Trieste Section of INFN, 34127 Trieste, Italy
- ²⁶ Abdus Salam ICTP, 34151 Trieste, Italy
- ²⁷ University of Turin, Department of Physics, 10125 Turin, Italy
- ²⁸ University of Eastern Piedmont, 15100 Alessandria, Italy
- ²⁹ Torino Section of INFN, 10125 Turin, Italy
- ³⁰ National Centre for Nuclear Research, 00-681 Warsaw, Poland^r
- ³¹ University of Warsaw, Faculty of Physics, 00-681 Warsaw, Poland^r
- ³² Warsaw University of Technology, Institute of Radioelectronics, 00-665 Warsaw, Poland^r
- ³³ Yamagata University, Yamagata, 992-8510 Japanⁿ
- ^a Also at Instituto Superior Técnico, Universidade de Lisboa, Lisbon, Portugal
- ^b Also at Department of Physics, Pusan National University, Busan 609-735, Republic of Korea and at Physics Department, Brookhaven National Laboratory, Upton, NY 11973, U.S.A.
- ^c Supported by the DFG Research Training Group Programme 1102 “Physics at Hadron Accelerators”
- ^d Also at Chubu University, Kasugai, Aichi, 487-8501 Japanⁿ
- ^e Also at KEK, 1-1 Oho, Tsukuba, Ibaraki, 305-0801 Japan
- ^f Present address: Universität Bonn, Helmholtz-Institut für Strahlen- und Kernphysik, 53115 Bonn, Germany
- ^g Also at Moscow Institute of Physics and Technology, Moscow Region, 141700, Russia
- ^h present address: RWTH Aachen University, III. Physikalisches Institut, 52056 Aachen, Germany
- ⁱ Supported by the German Bundesministerium für Bildung und Forschung
- ^j Supported by Czech Republic MEYS Grants ME492 and LA242
- ^k Supported by SAIL (CSR), Govt. of India
- ^l Supported by CERN-RFBR Grants 08-02-91009 and 12-02-91500
- ^m Supported by the Portuguese FCT - Fundação para a Ciência e Tecnologia, COMPETE and QREN, Grants CERN/FP/109323/2009, CERN/FP/116376/2010 and CERN/FP/123600/2011
- ⁿ Supported by the MEXT and the JSPS under the Grants No.18002006, No.20540299 and No.18540281; Daiko Foundation and Yamada Foundation
- ^o Supported by the DFG cluster of excellence ‘Origin and Structure of the Universe’ (www.universe-cluster.de)
- ^p Supported by EU FP7 (HadronPhysics3, Grant Agreement number 283286)
- ^q Supported by the Israel Science Foundation, founded by the Israel Academy of Sciences and Humanities
- ^r Supported by the Polish NCN Grant DEC-2011/01/M/ST2/02350
- * Deceased

1 Introduction

The Okubo-Zweig-Iizuka (OZI) rule [1] was formulated in the early days of the quark model, stating that all hadronic processes with disconnected quark lines are suppressed. It qualitatively explains phenomena like suppression of ϕ meson decays into non-strange particles and suppression of exclusive ϕ production in non-strange hadron collisions. Using the known deviation from the ideal mixing angle of the vector mesons ω and ϕ , $\delta_V = 3.7^\circ$, the production cross section of ϕ with respect to that of ω should be suppressed according to $\sigma(AB \rightarrow X\phi)/\sigma(AB \rightarrow X\omega) = \tan^2 \delta_V = 0.0042$, where A , B and X are non-strange hadrons [2]. At low energies, where baryonic and mesonic degrees of freedom are most relevant, the ratio can be expressed in terms of meson-meson or meson-nucleon couplings: $g_{\phi\rho\pi}^2/g_{\omega\rho\pi}^2 = g_{\phi NN}^2/g_{\omega NN}^2 = \tan^2 \delta_V = 0.0042$, where N denotes the nucleon. This is valid provided the coupling ratios $g_{\phi\rho\pi}/g_{\omega\rho\pi}$ and $g_{\phi NN}/g_{\omega NN}$ are equal as advocated in Ref. [3].

The OZI rule was tested in several experiments and is remarkably well fulfilled in many reactions (for a review, see *e.g.* Refs. [4] and [5]). Apparent violations of the OZI rule – observed in $p\bar{p}$ annihilations at rest and in nucleon-nucleon collisions – can be interpreted either as a true violation due to gluonic intermediate states (see *e.g.* Ref. [6]) or as an evasion from the OZI rule because of a hidden strangeness component in the nucleon [7]. Such a strangeness component, possibly polarised, was suggested as an explanation of the apparent OZI violations observed in $pN \rightarrow NpV$, $V = \omega, \phi$ by the SPHINX collaboration [8]. Large OZI violations at low energies have also led to speculations about crypto-exotic baryon resonances decaying to $N\phi$ [9].

Although being phenomenological in its origin, the OZI rule has been connected to QCD [2]. In a field theoretical approach to the OZI rule, a perturbative treatment based on quark-gluon degrees of freedom requires the scale of a specific process to be much larger than the QCD cut-off parameter $\Lambda_{QCD} \approx 200 \text{ MeV}/c$. In charmonium production, where the scale is governed by the charm quark current mass $m_c \approx 1275 \text{ MeV}/c^2$, the quark-antiquark pair is generated by gluon splitting, $g \rightarrow c\bar{c}$. This is in contrast to the case of strangeness production, where the scale corresponds to the strange quark current mass $m_s \approx 95 \text{ MeV}/c^2$, which is close to Λ_{QCD} . The validity of the quark-gluon picture can thus be questioned, and the relevant degrees of freedom need to be determined. Gluon splitting can only be used in an effective sense. This has also been discussed in connection to hyperon production in $\bar{p}p \rightarrow \bar{\Lambda}\Lambda$ production near threshold, where neither meson exchange models nor quark-gluon models give a complete explanation of the experimental data [10]. However, probed at virtualities Q^2 or $p_\perp^2 \gg 1 (\text{GeV}/c)^2$, which are large compared to $(2m_s)^2 c^2 \approx \Lambda_{QCD}^2 \approx 0.04 (\text{GeV}/c)^2$, the process can be described in the quark-gluon picture and we expect strangeness suppression to disappear, restoring flavour SU(3) symmetry.

In this work, we present an attempt to understand the effective scale governing the (hidden) strangeness production in the exclusive process $pp \rightarrow p\phi p$ by studying the degree of OZI violation. The difficulty lies in the separation of different reaction mechanisms as a function of transferred energy and angular momentum. The latter is reflected in the anisotropy of the decay angular distributions which can be expressed *via* the spin density matrix [11]. In the analysis of data from an unpolarised beam impinging on an unpolarised target, symmetries leave one independent element of the spin density matrix, ρ_{00} , which is a measure for spin alignment (tensor polarisation). It can be extracted from distributions of the angle between the decay plane (3-body decay) or decay axis (2-body decay) of the vector meson and a well-chosen reference axis [12].

The MOMO collaboration measured ρ_{00} of the ϕ meson in $pd \rightarrow {}^3\text{He}\phi$ near the kinematic threshold and the result was consistent with a complete alignment of the ϕ meson with respect to the incoming beam [13]. This is in sharp contrast to the case of the ω meson, which is produced unaligned at the same excess energy and in the same initial state, as found by the WASA collaboration [14]. The alignment of the ω meson in pp collisions was measured close to threshold by the COSY-TOF collaboration [16]

and in pN collisions at a beam momentum of $70 \text{ GeV}/c$ by SPHINX [15], whereas the ϕ alignment was measured at high energies by ACCMOR [17] and by STAR at RHIC [18]. Prior to our measurement, the only simultaneous measurement of ϕ and ω alignment using the same experimental set-up was performed by the SAPHIR collaboration [19, 20] in photoproduction.

At COMPASS, the exclusive reaction $p_{\text{beam}} p_{\text{target}} \rightarrow p_{\text{fast}} V p_{\text{recoil}}$ is measured at a beam momentum of $190 \text{ GeV}/c$. For simplicity, this will from now on be denoted $pp \rightarrow pVp$. Apart from this notation and unless otherwise stated explicitly, the symbol p without subscript and the Feynman variable $x_F = p_L/p_{L\text{max}}$, p_L denoting the longitudinal momentum, will refer to the fast proton. The reduced 4-momentum transfer squared t' from the beam to the recoil proton is defined as $t' = |t| - |t|_{\text{min}}$, where $t = (p_{p_{\text{beam}}} - (p_{p_{\text{fast}}} + p_V))^2$ and $|t|_{\text{min}}$ the minimum value of $|t|$.

For exclusive vector meson production, there are contributions from mainly two classes of processes: resonant and non-resonant production. First, resonant production means diffractive dissociation of the fast proton, where a Pomeron is emitted in the t -channel from the target and excites the beam particle (see Fig. 1, left panel). The target particle receives a small recoil but stays intact. The vector meson is then produced *via* a baryon resonance. On the other side, there is the non-resonant process including the case when a vector meson is radiated from the proton in the initial or final state. This is possible due to a finite coupling of the vector meson to the meson cloud of the nucleon [21]. These non-resonant processes are summarised in the middle panel of Fig. 1, where the blob in the upper vertex represents point-like and non-point-like interactions. Non-resonant vector meson production also includes central production where a Reggeon or Pomeron from the target and a Reggeon or Pomeron from the beam particle fuse in a central vertex (see Fig. 1, right panel). The production of ω and ϕ in Pomeron-Pomeron collisions does not conserve G -parity and is thus forbidden. Central Production is characterised by large rapidity gaps between all three final state particles. This is equivalent to large gaps between the x_F distributions of the outgoing particles. For the $pp \rightarrow pVp$ process this results in large x_F of the fast proton. Another special case of non-resonant production is the shake-out (see *e.g.* Ref. [7]) of a $q\bar{q}$ pair from the sea of one nucleon which becomes on-shell when interacting with a Pomeron from the other nucleon. In the case of shake-out, a rapidity gap is expected between the recoil particle and the other two particles, but not necessarily between the fast proton and the vector meson. Central production and shake-out can in this sense be considered as similar processes in two different regions of phase space.

The dynamics of the vector meson is determined by the incoming particles of the production vertex. In the case of Pomeron-Reggeon fusion and shake-out, the dynamics of the vector meson depends on the exchange object(s) while in resonant diffractive production, it depends on the intermediate resonance.

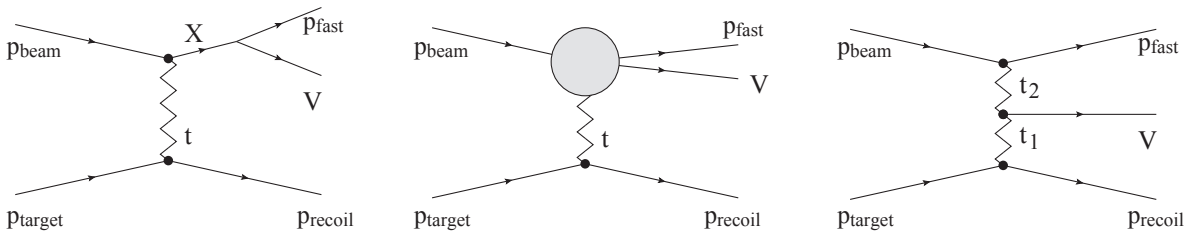


Fig. 1: Mechanisms for exclusive vector meson production at high energies. Left: Resonant single diffractive dissociation of the beam proton to a resonance X with subsequent decay. Middle: Non-resonant single diffractive excitation of the beam proton. The blob in the upper vertex denotes both point-like and non-point-like interactions. Right: Central production.

In this work, the cross section ratio

$$R_{\phi/\omega} = \frac{d\sigma(pp \rightarrow p\phi p)/dx_F}{d\sigma(pp \rightarrow p\omega p)/dx_F} \quad (1)$$

is presented as a function of x_F using different constraints on the invariant mass of proton and vector meson, M_{pV} . The data are in the kinematic domain $0 < p_{\perp}^2 < 1 (\text{GeV}/c)^2$. We also study the spin alignment of ω and ϕ and its dependence on x_F and M_{pV} in different reference frames.

2 Experimental set-up

The COMPASS experiment uses a fixed-target experiment situated at the M2 beam line of the CERN SPS. A detailed description can be found in Ref. [22]. For the present measurement, a beam of 190 GeV/c positively charged hadrons with a nominal intensity of $5 \cdot 10^6 \text{ s}^{-1}$ and a spill length of 10 s every 45 s was used. The positive beam is composed of 74.6% protons, 24.0% pions and 1.4% kaons. Each beam particle is identified using two differential Cherenkov detectors (CEDAR) and its trajectory is measured with a silicon microstrip telescope in front of the target.

The liquid hydrogen target with a length of 400 mm and a diameter of 35 mm is surrounded by two cylindrical layers of scintillators (RPD) for time-of-flight and dE/dx measurements of the slow target-recoil protons. The material of the target, the vacuum pipe and the inner layer of the RPD imply a minimum momentum transfer squared of $|t| = 0.07 (\text{GeV}/c)^2$ for detection of recoil protons.

The other final state particles are detected in a two-stage open forward spectrometer with large acceptance in momentum and angle. The small acceptance gap between the RPD and the forward spectrometer is covered by a lead-scintillator sandwich detector used as veto. The first and second spectrometer stage consists of a dipole magnet surrounded by tracking detectors followed by electromagnetic (ECAL1 and ECAL2) and hadron calorimeters. The first stage also contains a ring-imaging Cherenkov counter (RICH) for pion/kaon separation up to 50 GeV/c. Using C_4F_{10} as radiator gas, thresholds of 2.5 GeV/c and 9 GeV/c are obtained for pions and kaons, respectively.

The trigger system selects interactions in the target material by requiring a recoil proton in addition to an incoming beam particle. These requirements avoid any influence of the trigger onto the selection of particles in the forward spectrometer.

3 Analysis

3.1 Event selection

The results presented in this paper are obtained by selecting ω and ϕ mesons from the reactions $pp \rightarrow p\omega p$, $\omega \rightarrow \pi^+\pi^-\pi^0$ and $pp \rightarrow p\phi p$, $\phi \rightarrow K^+K^-$, respectively. The data were taken in 2008 and 2009 and correspond to an integrated luminosity of about 0.9 pb^{-1} .

Exactly one well-defined interaction vertex is required to be reconstructed within the target volume, for which the total charge of the three outgoing charged tracks is +1. The incoming beam particle must be identified as a proton in the CEDAR detectors. Furthermore, only events with exactly one proton detected in the RPD are selected.

For the selection of a π^0 in the $\omega \rightarrow \pi^+\pi^-\pi^0$ channel, at least two photon candidates are required, defined as neutral clusters in ECAL1 or ECAL2 with no associated reconstructed tracks. Energy thresholds of 1 GeV and 2 GeV are applied to ECAL1 and ECAL2, respectively. Furthermore, we require a photon pair in each event with invariant mass within a window around the π^0 PDG value, which corresponds to $\pm 2\sigma_{\text{ECAL}}$, where σ_{ECAL} is the mass resolution of a photon pair in the calorimeter. The momentum of the π^0 is then recalculated using a fit constrained to the PDG π^0 mass value to improve the resolution. The π^+ must be identified in the RICH detector. The separation of kaons and pions is done *via* a log-likelihood method. The likelihood for a pion hypothesis for the measured particle is required to be larger than the likelihood for all other possible particle assignments. Furthermore, RICH efficiencies are used to correct the particle yields. The sum of energies of the final state particles detected in the spectrometer

must be within a window of ± 5 GeV around the beam energy of 191 GeV, referred to in the following as exclusivity condition. The azimuthal angle of the forward going system ($\pi^+\pi^-\pi^0$ and the fast proton) and the azimuthal angle of the recoil proton must differ by 180° within a window of $\pm 16^\circ$ (coplanarity), which corresponds to twice the angular resolution of the RPD.

For the selection of ϕ mesons, the K^+ must be identified in the RICH detector. Kaons are identified within a smaller momentum range than pions by the RICH which imposes a momentum cut of about $10 - 50$ GeV/ c on kaons and influences the acceptance (see Sec. 3.2). In order to accept a measured particle as a kaon, the likelihood for the kaon hypothesis must be 1.3 times larger than the likelihood obtained by any other possible particle assignment including background. Again, RICH efficiencies are used to correct the particle yields. Exclusivity and coplanarity are required as in the case of $\pi^+\pi^-\pi^0$.

The reduced four-momentum transfer squared t' is limited to values larger than 0.1 (GeV/ c)² due to the RPD acceptance. The invariant mass of the system pV , denoted as M_{pV} , is constrained to 1.8 GeV/ c^2 $< M_{p\omega} < 4.0$ GeV/ c^2 and 2.1 GeV/ c^2 $< M_{p\phi} < 4.5$ GeV/ c^2 .

3.2 Acceptance

The spectrometer acceptance is accounted for by using a Monte Carlo (MC) based multi-dimensional correction. The Monte Carlo event generator assumes the two-step process $pp \rightarrow p_{\text{recoil}}X$, $X \rightarrow pV$, where the intermediate resonance X decays to the fast proton p and the vector meson V according to phase space and where the t' dependence of $\exp(-6.5t')$ and the minimum $t' = 0.07$ (GeV/ c)² are taken from real data. The Monte Carlo events are generated in narrow bins in M_X , *i.e.* the mass of X , and the total generated M_X range covers the COMPASS spectrometer acceptance. A beam parameterisation obtained from real data is used as input to the generator in order to achieve realistic beam conditions, including horizontal and vertical divergence of the beam for any given position of the interaction vertex.

The propagation of the generated particles and their decay products through the COMPASS spectrometer is simulated by the software package COMGEANT based on GEANT3 [23]. The efficiency and purity of the RICH detector are parameterised using real data, for details see Ref. [24]. In order to achieve a model independent correction, we use a three-dimensional acceptance matrix in t' , M_{pV} and x_F of the fast proton. Each K^+K^- or $\pi^+\pi^-\pi^0$ event from the collected data set is weighted by the corresponding entry in the three-dimensional cell (t' , M_{pV} and x_F) of the acceptance matrix. In a different approach, the results are re-calculated using a different acceptance matrix where x_F is replaced by $\cos\theta$, with θ being the helicity angle of the pV system as defined in Sec. 5.1. The results differ by less than 1%. The statistical uncertainty of each value of the acceptance matrix stems from a binomial probability density function as described in Ref. [25]. It is typically 3–5 times smaller than the statistical error from the real data and hence neglected.

The upper panels of Fig. 2 depict the x_F projection of the acceptance matrix for both final states. While the acceptance remains sizeable for $\pi^+\pi^-\pi^0$ down to $x_F = 0.2$, it changes more rapidly for K^+K^- due to the RICH detector. The analysis is therefore restricted to $0.6 < x_F < 0.9$ in both channels in order to compare ϕ and ω production within the same kinematic range. The impact of the acceptance correction on the uncorrected x_F distributions for vector meson, recoil and fast proton (shown in the middle panels of Fig. 2) is seen in the corresponding acceptance-corrected distributions (shown in the lower panels of Fig. 2). Note, that the latter only contain events for $0.6 < x_F < 0.9$, as described above. Note the clear peaks for high $x_F(p_{\text{fast}})$ and small $x_F(\phi)$ distributions, indicating a contribution from central production.

3.3 Background subtraction

The yield of ϕ mesons is determined from a fit of a Breit-Wigner shape with fixed width taken from Ref. [26], which is convoluted with a Gaussian on top of a background parameterisation that includes

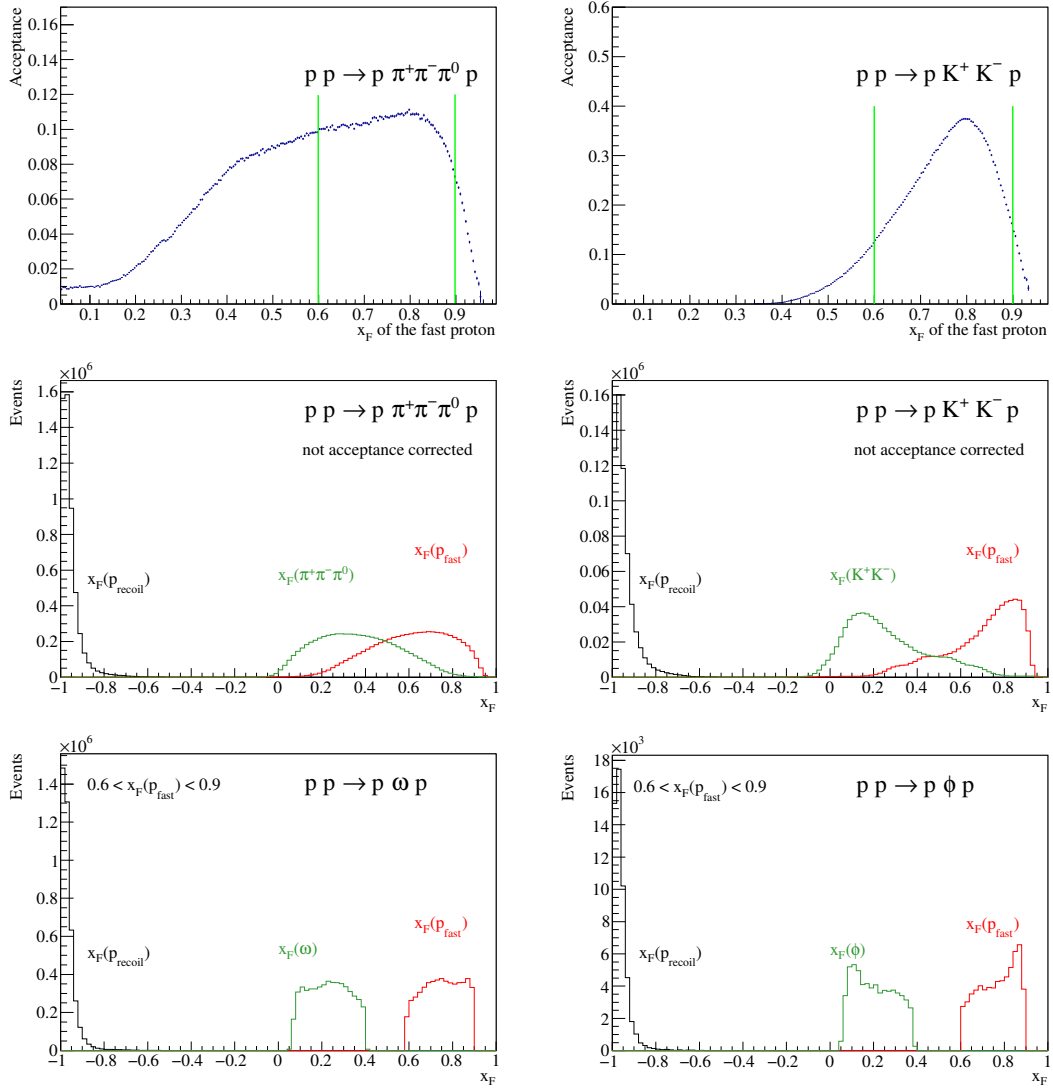


Fig. 2: Upper panels: One-dimensional (integrated) acceptances for $pp \rightarrow pp\omega, \omega \rightarrow \pi^+\pi^-\pi^0$ (left) and $pp \rightarrow pp\phi, \phi \rightarrow K^+K^-$ (right) as a function of x_F of the fast proton. Cuts used in the later analysis are illustrated by the vertical lines. Middle panels: x_F distributions for $pp \rightarrow pp\omega, \omega \rightarrow \pi^+\pi^-\pi^0$ (left) and $pp \rightarrow pp\phi, \phi \rightarrow K^+K^-$, acceptance uncorrected. Lower panels: The same as shown in the middle panels, but acceptance corrected and for $0.6 < x_F < 0.9$.

KK threshold effects. We observe a better fit quality using the simple Breit-Wigner functional form instead of also taking into account L -dependent centrifugal barrier terms. All results in this work are therefore obtained using the simpler Breit-Wigner function. The used background distribution function is $a(m_{K\bar{K}} - m_1)^n (m_{K\bar{K}} - m_2)^k$, where a, m_1, m_2, n and k are the fit parameters.

The yield of ω mesons is determined from a fit of a Breit-Wigner shape as explained above, but this time convoluted with two Gaussians to account for different resolutions of the two electromagnetic calorimeters. This fit also includes a second-degree polynomial background. Examples of mass spectra for the $0.6 < x_F < 0.7$ region are shown in Fig. 3.

The sideband subtraction is also used in order to estimate the systematics of the background subtraction. To obtain background corrected distribution of *e.g.* M_{pV} , events within $\pm 3\sigma$ of the $M_{\pi^+\pi^-\pi^0}$ or $M_{K^+K^-}$ distributions are taken and events in the sidebands from $\pm 4\sigma$ to $\pm 7\sigma$, respectively, are subtracted. The systematic uncertainty from the background subtraction is estimated by comparing the yields obtained

using different parameterisations of peak and background. The relative difference of the yields is found to be always below 5%.

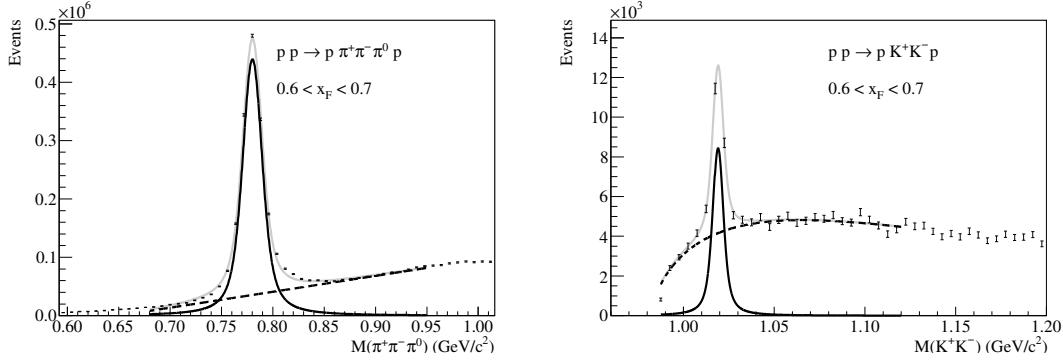


Fig. 3: Left: The fitted mass distribution of the $\pi^+\pi^-\pi^0$ system where the x_F of the fast proton is within the interval $0.6 < x_F < 0.7$. Right: The fitted mass distribution of the K^+K^- system in the $0.6 < x_F < 0.7$ range. The signal fit is shown in black, the background is shown by the dashed curve and their sum is shown in grey.

3.4 Systematic uncertainties

In addition to the uncertainty of the background subtraction, there are other effects which contribute to the overall systematic uncertainties. Most efficiencies (CEDAR, RPD, track reconstruction) cancel in $R_{\phi/\omega}$. Systematic effects introduced by the MC generator are negligible since a multi-dimensional acceptance correction is applied (see section 3.2). The uncertainty from the RICH is estimated to be 5% on $R_{\phi/\omega}$ and dominantly stems from background subtraction uncertainties in the RICH efficiency determination. The photon reconstruction efficiency of the ECALs is determined by comparing ω decays into $\pi^+\pi^-\pi^0$ and $\pi^0\gamma$ in both real data and MC data with the assumption that the π^0 efficiency is the same in both channels. The deviation between measured efficiency and MC efficiency is found to be below 10% and used as an upper limit for the systematic uncertainty arising from the ECALs. The quadratic sum of the 5% uncertainty from the background subtraction, the 5% from the RICH efficiency and the 10% from the photon reconstruction efficiency results in a total systematic uncertainty of 12% for the results on the cross section ratio quoted in Sec. 4.2.

Uncertainties due to RICH and ECAL efficiencies have no impact on the shape of angular distributions (Sec. 5) and M_{pV} distributions and thus are neglected. Hence, only the 5% uncertainty due to background subtraction is relevant.

4 M_{pV} distributions and cross section ratio $R_{\phi/\omega}$

4.1 Mass M_{pV} of the system of fast proton and vector meson

The acceptance-corrected invariant mass distributions of the pV system are shown in Fig. 4. In the case of ω , where the background is small compared to the signal (see Fig. 3) and has a locally linear behaviour near the ω peak, the distributions are obtained using a sideband subtraction as explained in Sec. 3.4. In the $M_{p\omega}$ spectrum shown to the left in Fig. 4 several structures on top of a smooth continuum are clearly discernible. After dividing the ω data into finer bins in x_F , as in Fig. 5, the structures appear even clearer. In the absence of a partial wave analysis, which is beyond the scope of this paper, the bumps are compared with known N^* resonances. The high-mass bumps are consistent with resonances listed in the PDG [26]: the one at about $2.2 \text{ GeV}/c^2$ with $N^*(2190) J^P = \frac{7}{2}^-$, $N^*(2200) J^P = \frac{9}{2}^+$ and $N^*(2250) J^P = \frac{9}{2}^-$ and the one at about $2.6 \text{ GeV}/c^2$ with $N^*(2600) J^P = \frac{11}{2}^-$ and $N^*(2700) J^P = \frac{13}{2}^+$. These prominent resonances have high spin.

The $p\phi$ mass spectrum (Fig. 4, right panel) is obtained using a fit for background subtraction, as explained in Section 3.3. It appears without pronounced structures, also consistent with earlier findings [26].

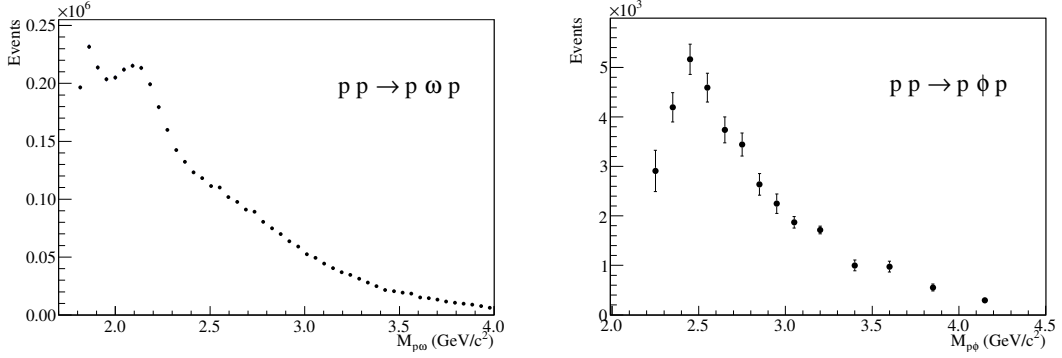


Fig. 4: Distributions of the invariant mass of the pV system for $0.6 < x_F < 0.9$. Left: The $M_{p\omega}$ spectrum. The background is subtracted using the sideband method. Right: The $M_{p\phi}$ spectrum. The background is subtracted using a polynomial fit described in Section 3.3 and the uncertainty from the fit is included in the error bars.

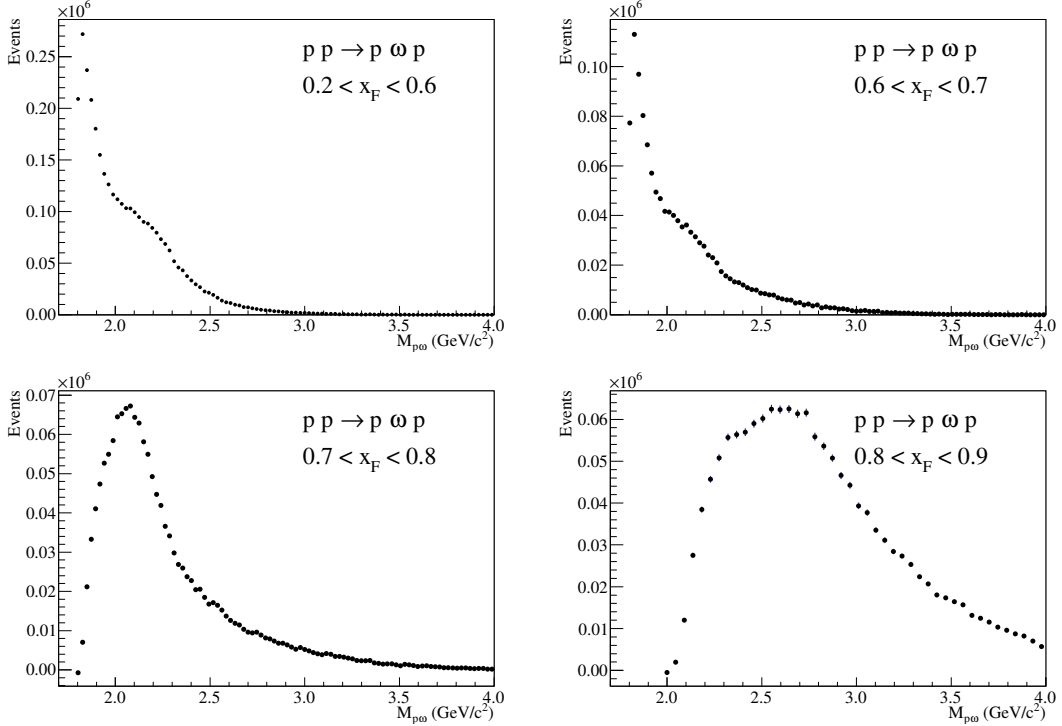


Fig. 5: Distributions of the mass of the $p-\omega$ system for $0.2 < x_F < 0.6$ (upper left), $0.6 < x_F < 0.7$ (upper right), $0.7 < x_F < 0.8$ (lower left) and $0.8 < x_F < 0.9$ (lower right).

4.2 Cross section ratio $R_{\phi/\omega}$

The $\pi^+\pi^-\pi^0$ and K^+K^- data are divided into three intervals of x_F : 0.6–0.7, 0.7–0.8 and 0.8–0.9. In each interval, the acceptance-corrected ω and ϕ yields are calculated using the method described in Sec. 3.3 and corrected for the branching ratios of the $\omega \rightarrow \pi^+\pi^-\pi^0$ and $\phi \rightarrow K^+K^-$ decays, respectively. The ratio $R_{\phi/\omega}$ is calculated in each x_F interval. The results, summarised in Table 1 and Fig. 6, show that the OZI rule is violated by a factor F_{OZI} of 4.5, 4.0 and 2.9, *i.e.* ϕ production is enhanced with respect to the OZI rule prediction. The violation factor is defined as $F_{\text{OZI}} = R_{\phi/\omega} / \tan^2 \delta_V$, with $\tan^2 \delta_V = 0.0042$ being the OZI prediction. It is notable that the violation is smaller in the highest x_F bin. The average

value $\langle R \rangle_{\phi/\omega} = 0.0160 \pm 0.0003 \pm 0.0020$ is consistent with the result from SPHINX [8], which is $\langle R \rangle_{\phi/\omega} = 0.0155 \pm 0.0005 \pm 0.0031$.

Table 1: Differential cross section ratios $R_{\phi/\omega} = \frac{d\sigma(pp \rightarrow p\phi p)/dx_F}{d\sigma(pp \rightarrow p\omega p)/dx_F}$ and corresponding OZI violation factors F_{OZI} .

x_F	$R_{\phi/\omega}$	Stat.	Fit	Syst.	F_{OZI}
0.6–0.7	0.019	0.0003	0.0006	0.0023	4.5 ± 0.6
0.7–0.8	0.017	0.0002	0.0004	0.002	4.0 ± 0.5
0.8–0.9	0.012	0.0002	0.0005	0.0014	2.9 ± 0.4

The $M_{p\omega}$ distributions shown in Fig. 5 indicate that the $pp \rightarrow p\omega p$ cross section may be heavily influenced by the baryon resonances. Unless the resonant contribution is removed from the data set, a measurement of the cross section ratio $R_{\phi/\omega}$ does not give sufficient information, neither about the strangeness content of the nucleon nor about other production mechanisms than resonant diffractive production. No resonances are visible above $M_{p\omega} = 3.3 \text{ GeV}/c^2$. For a consistent treatment of ϕ and ω production, the vector meson momentum p_V is used as determined in the pV rest system:

$$p_V = \frac{\sqrt{\left(M_{pV}^2 - (m_V + m_p)^2\right) \left(M_{pV}^2 - (m_V - m_p)^2\right)}}{2M_{pV}}. \quad (2)$$

The mass value $M_{p\omega} = 3.3 \text{ GeV}/c^2$ corresponds to $p_V = 1.4 \text{ GeV}/c$, which is hence used as a cut value also for the ϕ meson. The requirement of $p_V > 1.4 \text{ GeV}/c$ results in ratios of 0.034 and 0.032 in the two bins $0.7 < x_F < 0.8$ and $0.8 < x_F < 0.9$, respectively, which correspond to OZI violation factors $F_{\text{OZI}} = 7.9$ and $F_{\text{OZI}} = 7.6$. In the bin $0.6 < x_F < 0.7$, the ϕ yield is insufficient for a reliable $R_{\phi/\omega}$ estimate. Detailed results are summarised in the bottom part of Table 2 and in Fig. 6.

Note that if the low-mass resonant region in $M_{p\omega}$ is removed, this results in an OZI violation factor of about 8, independent of x_F in the observed range. This agrees well with the results from the SPHINX experiment that operated at a beam energy of 70 GeV [8]. In order to remove the resonant region, SPHINX applied a weaker cut of 1 GeV/c on the p_V momentum. This corresponds to mass values of $M_{p\omega}$ of 2.64 GeV/c² and $M_{p\phi}$ of 2.8 GeV/c². Applying the same cut on the COMPASS data gives ratios $R_{\phi/\omega} = 0.032, 0.038$ and 0.019 in the three x_F bins, which correspond to OZI violation factors $F_{\text{OZI}} = 7.6, 9$ and 4.5 respectively, as summarised in the top part of Table 2 and Fig. 6. The COMPASS results below $x_F = 0.8$ are consistent with the SPHINX result $\frac{\sigma(pN \rightarrow pN\phi)}{\sigma(pN \rightarrow pN\omega)} = 0.040 \pm 0.0004 \pm 0.008$. The x_F range of the SPHINX data is not stated explicitly in Ref. [8].

Table 2: Differential cross section ratio $R_{\phi/\omega}$ and corresponding OZI violation factors F_{OZI} for different p_V cuts.

p_V (GeV/c)	x_F	$R_{\phi/\omega}$	Stat.	Fit	Syst.	F_{OZI}
> 1.0	0.6–0.7	0.032	0.0007	0.0013	0.0038	7.6 ± 1.0
> 1.0	0.7–0.8	0.038	0.0006	0.0010	0.0046	9.0 ± 1.1
> 1.0	0.8–0.9	0.019	0.0003	0.0005	0.0023	4.5 ± 0.6
> 1.4	0.7–0.8	0.033	0.0013	0.0025	0.0040	7.9 ± 1.1
> 1.4	0.8–0.9	0.032	0.0011	0.0017	0.0038	7.6 ± 1.0

5 Results on spin alignment

In order to get more information about production mechanisms, in particular to find out whether they are the same or different for ω and ϕ , it is helpful to study the spin-alignment (tensor polarisation) of the

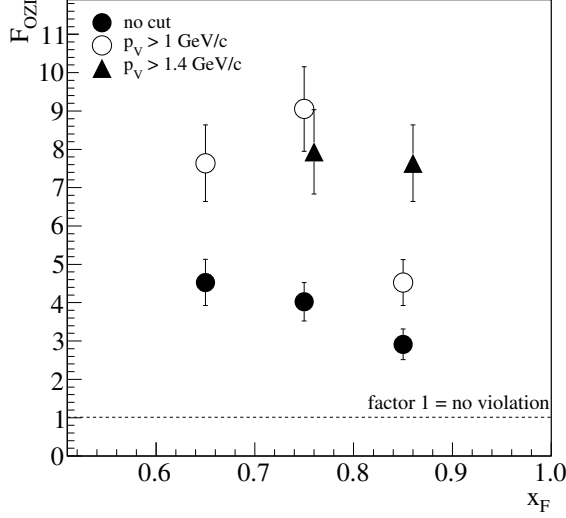


Fig. 6: OZI violation factor F_{OZI} as a function of x_F for different p_V cuts.

produced vector mesons with respect to a given quantisation axis. For different production processes, the preferential axis of alignment of the vector meson may be different. In this section, we study the spin alignment by determining the distributions of the angle between the analyser, defined by the direction of the decay particles of the vector meson, and two different quantisation axes.

In the 3-body decay of the ω meson, the normal to the decay plane is the most sensitive analyser [27]. In the case of a vector meson decaying into two pseudoscalars, *e.g.* $\phi \rightarrow K^+ K^-$, one chooses the momentum vector of either one. Schilling, Seyboth and Wolf [12] describe the strong decay of a spin-one particle into either two or three pseudoscalars in terms of the spin-density matrix ρ and the decay matrix T , obtaining the following angular distribution:

$$\begin{aligned}
 W(\cos\theta, \phi) &= \text{Tr}\{T^* \rho T\} \\
 &= \frac{3}{8\pi} \left(\rho_{11} \sin^2\theta + \rho_{00} \cos^2\theta - \sqrt{2}\rho_{10} \sin 2\theta \cos\phi - \rho_{1-1} \sin^2\theta \cos 2\phi \right). \quad (3)
 \end{aligned}$$

Integrating over the azimuthal angle ϕ , and using $\text{Tr}\{\rho\} = 1 = \rho_{00} + \rho_{11} + \rho_{-1-1}$ combined with the symmetry requirement $\rho_{11} = \rho_{-1-1}$ simplifies Eq. (3) to:

$$W(\cos\theta) = \frac{3}{4} \left(1 - \rho_{00} + (3\rho_{00} - 1) \cos^2\theta \right). \quad (4)$$

For $\rho_{00} = 1/3$, one obtains isotropic angular distributions. If $\rho_{00} = 0$, we have a $\sin^2\theta$ dependence and the vector mesons are in the magnetic sub-state $M = \pm 1$ with respect to the quantisation axis, while $\rho_{00} = 1$ gives a pure $\cos^2\theta$ dependence and corresponds to $M = 0$.

In the figures of this section, the error bars represent the quadratic sum of statistical uncertainty and the point-to-point uncertainty of the background subtraction.

5.1 Spin alignment with respect to the direction of the pV system

The spin alignment is first studied in the pV helicity frame. The reference axis (z -axis) is the direction of the pV system in the rest system of the vector meson V . If, on the one hand, the vector meson results from a diffractively produced baryon resonance, the spin alignment of the vector meson is expected to be sensitive to the direction of this resonance. If on the other hand the dominating process is a central Reggeon–Reggeon/Reggeon–Pomeron fusion or in the absence of a resonant system, there is no longer a

preferred reference axis and the distributions are expected to be isotropic. The polar angle of an analyser in the helicity frame will in the following be referred to as ‘‘helicity angle’’ and be denoted by θ_H . The $\cos^2\theta_H$ distributions are shown in Fig. 7 in different x_F intervals. The background distribution (open circles) is obtained by sideband subtraction and found to be isotropic. A striking feature of the signal data is that the slope is varying with x_F in the case of the ω meson (see Fig. 7, left), going from a strong negative slope in the interval $0.2 < x_F < 0.6$ passing through isotropy in the interval $0.7 < x_F < 0.8$ to a strong positive slope in the interval $0.8 < x_F < 0.9$. No such behaviour is observed in the case of the ϕ meson (see Fig. 7, right), for which the distributions are fairly isotropic in all three x_F intervals between 0.6 and 0.9. In the case of the ϕ meson, it should however be pointed out that the statistical uncertainty is significantly larger compared to the case of ω and it is difficult to draw definite conclusions from the ϕ decay angular distributions.

The ρ_{00} element is extracted by fitting straight lines $a + bx$, $x = \cos^2\theta_H$ to the data points and then solving Eq. 4. The fits were performed with and without including the leftmost and the rightmost data points in the angular distributions. The difference is included in the uncertainty. For ω , the contribution to the total uncertainty is very small. For ϕ it is typically between 5% and 10%. The fit results are shown in Table 3 and Fig. 8 including those for $p_\omega > 1 \text{ GeV}/c$. Within uncertainties, no ϕ meson spin alignment is observed with respect to the $p\phi$ direction. Similarly, the ω meson alignment with respect to the $p\omega$ direction almost vanishes for $p_\omega > 1 \text{ GeV}/c$ and $x_F < 0.8$. For $p_\omega > 1.4 \text{ GeV}/c$, above the low-mass resonant region, the angular distribution of the ω meson decay is, within the larger uncertainty, consistent with isotropy even when $x_F > 0.8$.

Table 3: Spin alignment ρ_{00} extracted from the helicity angle distributions for ϕ and ω production, in the latter case with various cuts on p_ω . The uncertainty is the propagated uncertainty from the linear fits, which in turn includes the quadratic sum of statistical uncertainties and uncertainties from the background subtraction.

Reaction	x_F	ρ_{00}
$pp \rightarrow pp\phi, \phi \rightarrow K^+ K^-$	0.6–0.7	0.38 ± 0.03
$pp \rightarrow pp\phi, \phi \rightarrow K^+ K^-$	0.7–0.8	0.35 ± 0.02
$pp \rightarrow pp\phi, \phi \rightarrow K^+ K^-$	0.8–0.9	0.39 ± 0.04
$pp \rightarrow pp\omega, \omega \rightarrow \pi^+ \pi^- \pi^0$	0.2–0.6	0.232 ± 0.003
$pp \rightarrow pp\omega, \omega \rightarrow \pi^+ \pi^- \pi^0$	0.6–0.7	0.289 ± 0.004
$pp \rightarrow pp\omega, \omega \rightarrow \pi^+ \pi^- \pi^0$	0.7–0.8	0.330 ± 0.003
$pp \rightarrow pp\omega, \omega \rightarrow \pi^+ \pi^- \pi^0$	0.8–0.9	0.449 ± 0.003
$pp \rightarrow pp\omega, \omega \rightarrow \pi^+ \pi^- \pi^0, p_V > 1.0 \text{ GeV}/c$	0.2–0.6	0.30 ± 0.01
$pp \rightarrow pp\omega, \omega \rightarrow \pi^+ \pi^- \pi^0, p_V > 1.0 \text{ GeV}/c$	0.6–0.7	0.34 ± 0.01
$pp \rightarrow pp\omega, \omega \rightarrow \pi^+ \pi^- \pi^0, p_V > 1.0 \text{ GeV}/c$	0.7–0.8	0.306 ± 0.006
$pp \rightarrow pp\omega, \omega \rightarrow \pi^+ \pi^- \pi^0, p_V > 1.0 \text{ GeV}/c$	0.8–0.9	0.463 ± 0.003
$pp \rightarrow pp\omega, \omega \rightarrow \pi^+ \pi^- \pi^0, p_V > 1.4 \text{ GeV}/c$	0.8–0.9	0.37 ± 0.03

Extracting helicity angle distributions in slices of $M_{p\omega}$ reveals a clear dependence of ρ_{00} on $M_{p\omega}$, see Figs. 9 and 11 and Table 4. The dependence of ρ_{00} on x_F is connected to the ρ_{00} dependence on $M_{p\omega}$, as different intermediate baryon resonances with different masses dominate ω production in different x_F regions. The ω spin may hence be differently aligned with different mother baryons.

The $M_{p\phi}$ spectrum (see Fig. 4) does not show apparent structures and no baryon resonances are known to decay into $p\phi$ [26]. This is in line with the ρ_{00} results for ϕ , which are consistent with an unaligned ϕ with respect to a hypothetical intermediate baryon, fairly independent of x_F . The angular distribution extracted in two different $M_{p\phi}$ ranges are both consistent with isotropy. However, the errors are much larger than in the case of ω and a small alignment can therefore not be excluded. In order to compare the ρ_{00} values from ϕ and ω , we also extracted ρ_{00} for ω within the same x_F range and the corresponding

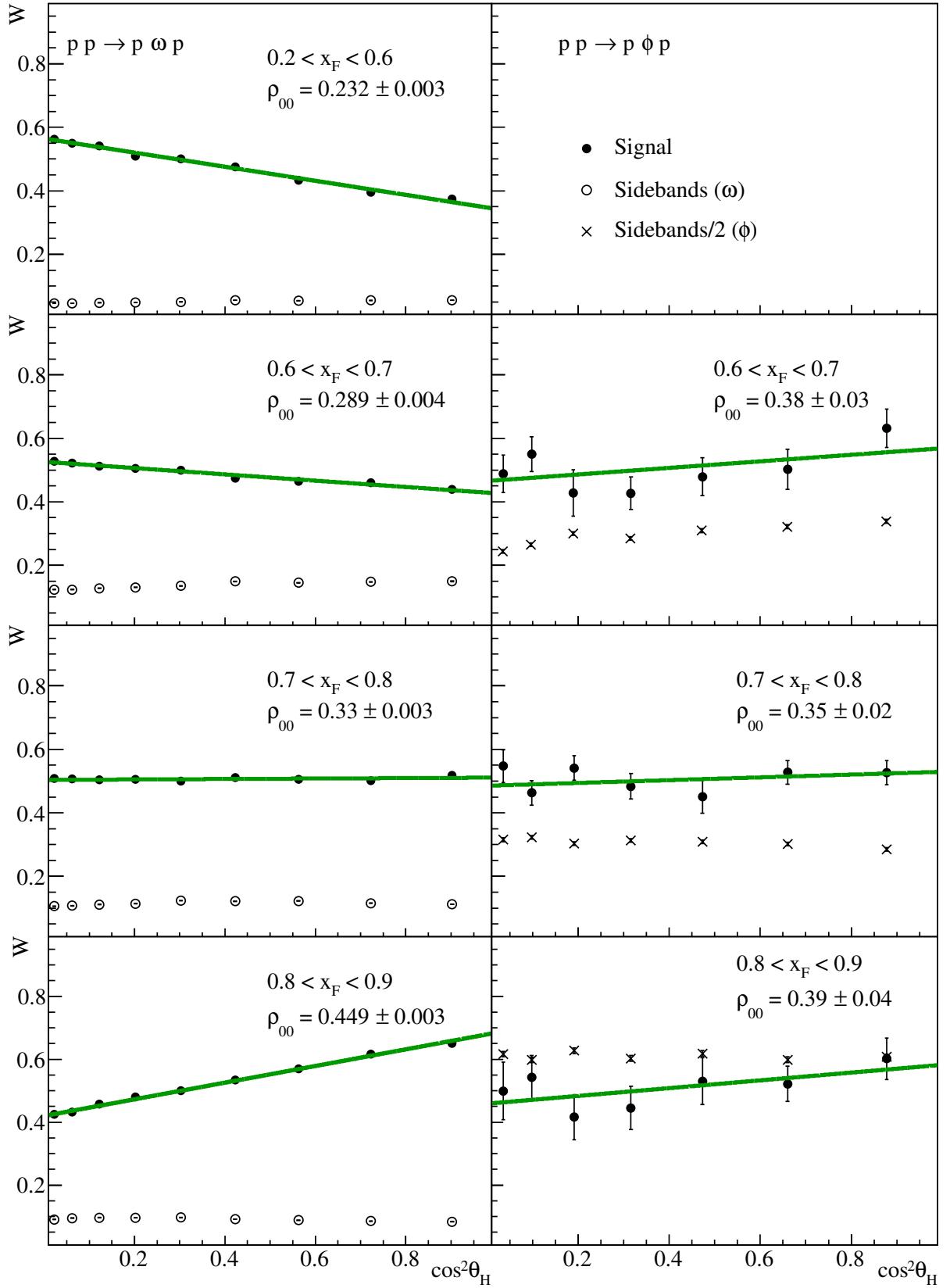


Fig. 7: The closed points represent the angular distributions of $\cos^2 \theta$, where $\theta = \theta_H$ is the helicity angle of the ω meson (right panels) and of the ϕ meson (left panels) in different x_F regions. The open points show the corresponding distribution for the events in the sidebands around the ω peak in the $M(\pi^+ \pi^- \pi^0)$ distribution. The crosses show the corresponding distribution (scaled by 0.5) for the events in the sidebands around the ϕ peak in the $M(K^+ K^-)$ distribution. The lines are the results of linear fits as explained in the text.

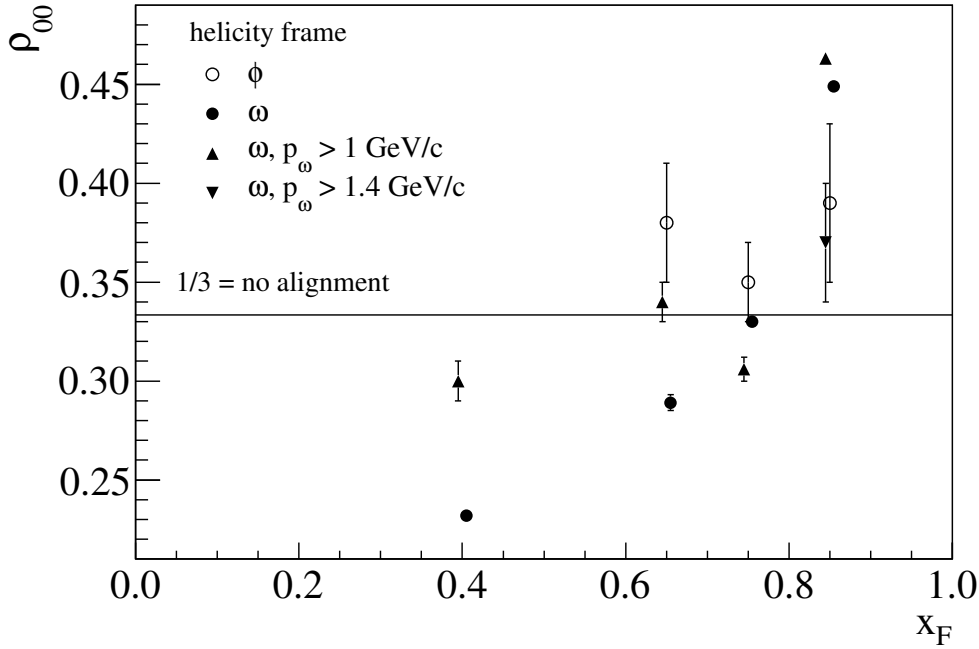


Fig. 8: Spin alignment ρ_{00} extracted from the helicity angle distributions for ϕ and ω production as a function of x_F for several cuts on p_V .

M_{pV} range as in the case of ϕ . In the last four lines of Table 4, the $M_{p\omega}$ and $M_{p\phi}$ ranges correspond to the same p_V (see Eq. 2) range. In the lower mass intervals, the ρ_{00} values agree within their combined errors, and the difference is significant in the higher mass interval. The high value of the cross section ratio, the absence of structures in the $M_{p\phi}$ distribution, the peaks in the x_F distributions in the lower-right panel of Fig. 2 and the close-to-isotropic angular distributions indicate that independent of $M_{p\phi}$ either a non-resonant diffractive process or a central process dominates ϕ production within our kinematical range. Since the COMPASS acceptance is small close to $M_{p\phi} = 2.1 \text{ GeV}/c^2$, no conclusions can be drawn concerning the crypto-exotic $p\phi$ resonance suggested in Ref. [9].

5.2 Spin alignment with respect to the transferred momentum

The isotropic $p\phi$ helicity angle distribution rises the question whether there is a more natural choice of reference axis, to which also centrally produced vector mesons are sensitive. Since both diffractive and central production processes involve the exchange of at least one Reggeon, we define a new reference axis by taking the direction of the momentum transfer from the beam proton in the initial state to the fast proton in the final state, denoted $\Delta\vec{P}$. In the rest system of the vector meson, this is opposite to the momentum transfer from the target to the recoil. In the case of central production, the dynamics of the vector meson should depend strongly on the exchange, whereas in resonant diffractive production it is instead inherited from the intermediate baryon resonance. The angle θ_{EX} is calculated in the rest system of the vector meson with the same analyser as before.

The results are shown in Fig. 12. The extracted values of ρ_{00} are presented in Table 5 and in Fig. 13. The angular distribution of the background (open circles / crosses) is isotropic, which demonstrates that the observed alignment in the signal region is a real physical effect and not an artefact introduced by the experiment. Both ϕ and ω mesons are aligned transverse to the direction of the exchanged Reggeon/Pomeron. The alignment is stronger when x_F increases. In production processes without an intermediate state or resonance, the vector meson will “remember” the direction of momentum transfer

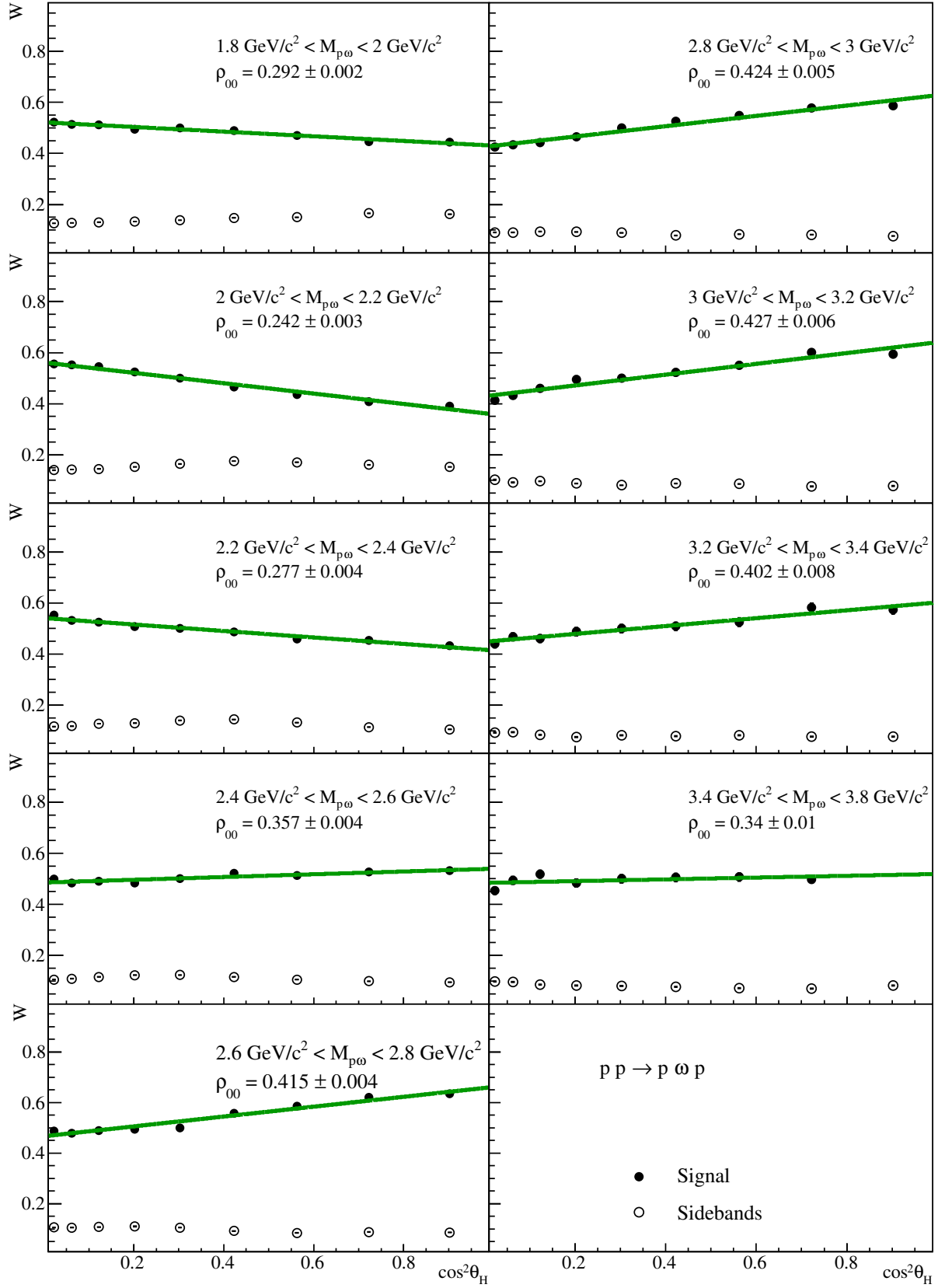


Fig. 9: Angular distributions of $\cos^2 \theta$, where $\theta = \theta_H$ is the helicity angle of the ω meson in different $M_{p\omega}$ regions. From top left to bottom right, mass ranges in GeV/c^2 : 1.8–2.0, 2.2–2.4, 2.4–2.6, 2.6–2.8, 2.8–3.0, 3.0–3.2, 3.2–3.4, 3.4–3.8. The open points show the corresponding distribution for the events in the sidebands around the ω peak in the $M(\pi^+\pi^-\pi^0)$ distribution. The lines are the results of linear fits as explained in the text.

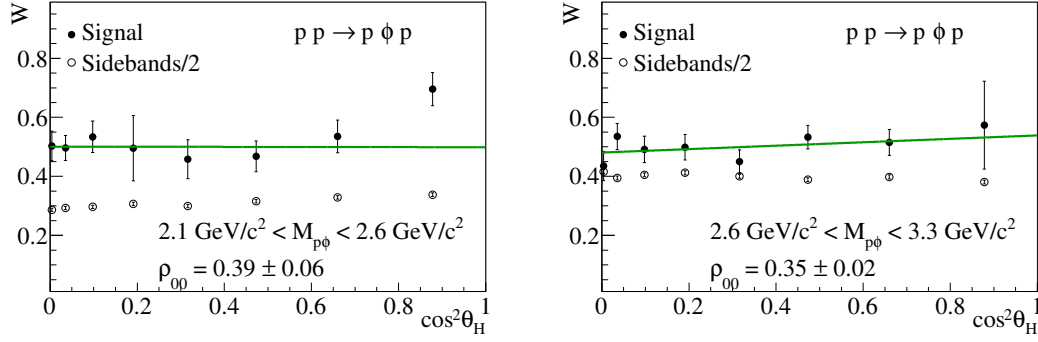


Fig. 10: Angular distributions of $\cos^2 \theta$, where $\theta = \theta_H$ is the helicity angle of the ϕ meson for $2.1 \text{ GeV}/c^2 < M_{p\phi} < 2.6 \text{ GeV}/c^2$ (left) and $2.6 \text{ GeV}/c^2 < M_{p\phi} < 3.3 \text{ GeV}/c^2$ (right). The open points show the corresponding distribution for the events in the sidebands around the ϕ peak in the $M(K^+K^-)$ distribution. The lines are the results of linear fits as explained in the text.

Table 4: Upper section: Spin alignment ρ_{00} extracted from the helicity angle distributions for ω production in the region $0.2 < x_F < 0.9$ for different $M_{p\omega}$ regions. Middle section: The same but for ϕ production in the range $0.6 < x_F < 0.9$. Lower section: The ρ_{00} values extracted for ω within $0.6 < x_F < 0.9$ and in the corresponding mass range as in the case of ϕ as explained in the text. The uncertainty is the propagated uncertainty from the linear fits, which in turn includes the quadratic sum of statistical uncertainties and uncertainties from the background subtraction.

Reaction	M_{pV} in GeV/c^2	ρ_{00}
$pp \rightarrow pp\omega, \omega \rightarrow \pi^+\pi^-\pi^0$	1.8–2.0	0.292 ± 0.002
$pp \rightarrow pp\omega, \omega \rightarrow \pi^+\pi^-\pi^0$	2.0–2.2	0.242 ± 0.003
$pp \rightarrow pp\omega, \omega \rightarrow \pi^+\pi^-\pi^0$	2.2–2.4	0.277 ± 0.004
$pp \rightarrow pp\omega, \omega \rightarrow \pi^+\pi^-\pi^0$	2.4–2.6	0.357 ± 0.004
$pp \rightarrow pp\omega, \omega \rightarrow \pi^+\pi^-\pi^0$	2.6–2.8	0.415 ± 0.004
$pp \rightarrow pp\omega, \omega \rightarrow \pi^+\pi^-\pi^0$	2.8–3.0	0.424 ± 0.005
$pp \rightarrow pp\omega, \omega \rightarrow \pi^+\pi^-\pi^0$	3.0–3.2	0.427 ± 0.006
$pp \rightarrow pp\omega, \omega \rightarrow \pi^+\pi^-\pi^0$	3.2–3.4	0.402 ± 0.008
$pp \rightarrow pp\omega, \omega \rightarrow \pi^+\pi^-\pi^0$	3.4–3.8	0.35 ± 0.01
$pp \rightarrow pp\phi, \phi \rightarrow K^+K^-$	2.1–2.6	0.39 ± 0.06
$pp \rightarrow pp\phi, \phi \rightarrow K^+K^-$	2.6–3.3	0.35 ± 0.02
$pp \rightarrow pp\omega, \omega \rightarrow \pi^+\pi^-\pi^0$	1.88–2.42	0.321 ± 0.002
$pp \rightarrow pp\omega, \omega \rightarrow \pi^+\pi^-\pi^0$	2.42–3.17	0.423 ± 0.002

of the incoming Pomeron, which in turn should influence the spin orientation of the vector meson. This is the case in central production and when the vector meson is produced by a shake-out of a $q\bar{q}$ object in the proton.

The alignment of the ω meson reaches a maximum in the region $0.7 < x_F < 0.8$ while it is slightly smaller in the $0.8 < x_F < 0.9$. The results for ω and ϕ show the same trend, namely increasing anisotropy with increasing x_F , and are consistent with each other within uncertainties after removing the low-mass resonant part of the ω data. This indicates that this reference axis is only weakly sensitive to diffractive (resonant and non-resonant) production and strongly sensitive to central production, as expected. Non-resonant diffractive production (middle panel of Fig. 1) may contribute at low and intermediate values of x_F while central production should dominate at high x_F .

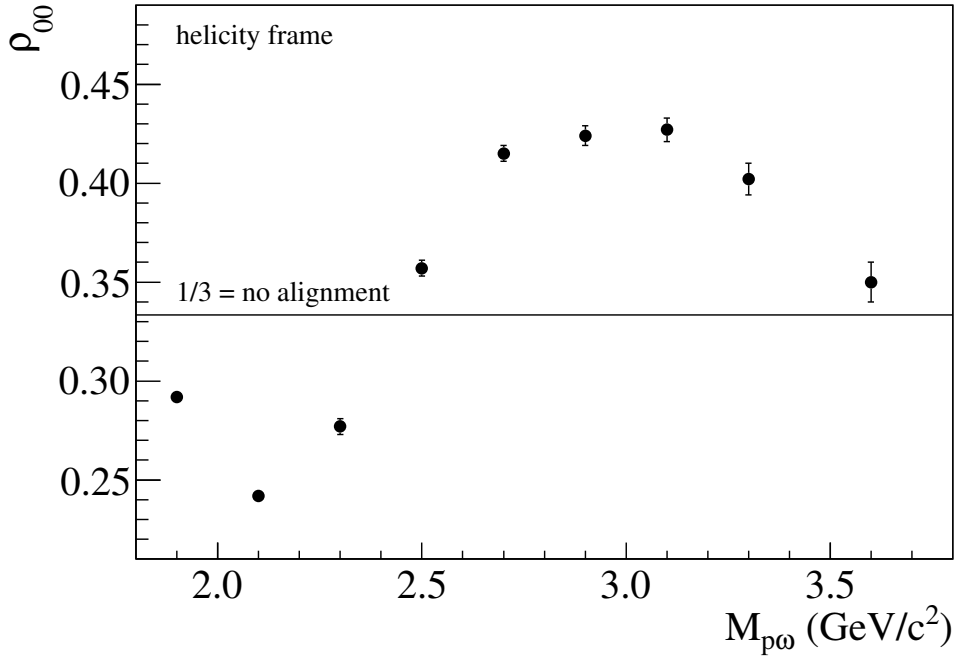


Fig. 11: Spin alignment ρ_{00} as a function of $M_{p\omega}$.

Table 5: Spin alignment ρ_{00} extracted using $\Delta\vec{P}$ as reference axis. The Table includes ϕ and ω production. The results for different p_V cuts are also given for ω . The uncertainty is the propagated uncertainty from the linear fits, which in turn includes the quadratic sum of statistical uncertainties and uncertainties from the background subtraction.

Reaction	x_F	ρ_{00}
$pp \rightarrow pp\phi, \phi \rightarrow K^+K^-$	0.6–0.7	0.51 ± 0.03
$pp \rightarrow pp\phi, \phi \rightarrow K^+K^-$	0.7–0.8	0.58 ± 0.02
$pp \rightarrow pp\phi, \phi \rightarrow K^+K^-$	0.8–0.9	0.67 ± 0.04
$pp \rightarrow pp\omega, \omega \rightarrow \pi^+\pi^-\pi^0$	0.2–0.6	0.408 ± 0.002
$pp \rightarrow pp\omega, \omega \rightarrow \pi^+\pi^-\pi^0$	0.6–0.7	0.492 ± 0.003
$pp \rightarrow pp\omega, \omega \rightarrow \pi^+\pi^-\pi^0$	0.7–0.8	0.582 ± 0.002
$pp \rightarrow pp\omega, \omega \rightarrow \pi^+\pi^-\pi^0$	0.8–0.9	0.572 ± 0.002
$pp \rightarrow pp\omega, \omega \rightarrow \pi^+\pi^-\pi^0, p_V > 1.0 \text{ GeV}/c$	0.6–0.7	0.39 ± 0.01
$pp \rightarrow pp\omega, \omega \rightarrow \pi^+\pi^-\pi^0, p_V > 1.0 \text{ GeV}/c$	0.7–0.8	0.527 ± 0.005
$pp \rightarrow pp\omega, \omega \rightarrow \pi^+\pi^-\pi^0, p_V > 1.0 \text{ GeV}/c$	0.8–0.9	0.577 ± 0.002
$pp \rightarrow pp\omega, \omega \rightarrow \pi^+\pi^-\pi^0, p_V > 1.4 \text{ GeV}/c$	0.8–0.9	0.601 ± 0.005

6 Discussion

An important process in exclusive ω meson production appears to be diffractive excitation of the beam proton with the excitation into nucleon resonances followed by a two-body decay $N^* \rightarrow p\omega$. This is supported by the structures in the $M_{p\omega}$ spectra in Figs. 4 and 5, which are consistent with known high-spin resonances [26], and the significant alignment of the ω meson with respect to the direction of the $p\omega$ system. The alignment is strongly dependent on $M_{p\omega}$. The N^* spin is aligned with its direction. In a two body decay, high spin resonances have to emit the vector meson with an orbital angular momentum, $\vec{J} = \vec{L} + \vec{J}_p + \vec{J}_V$. If the vector meson spin is preferentially aligned with the direction of the orbital

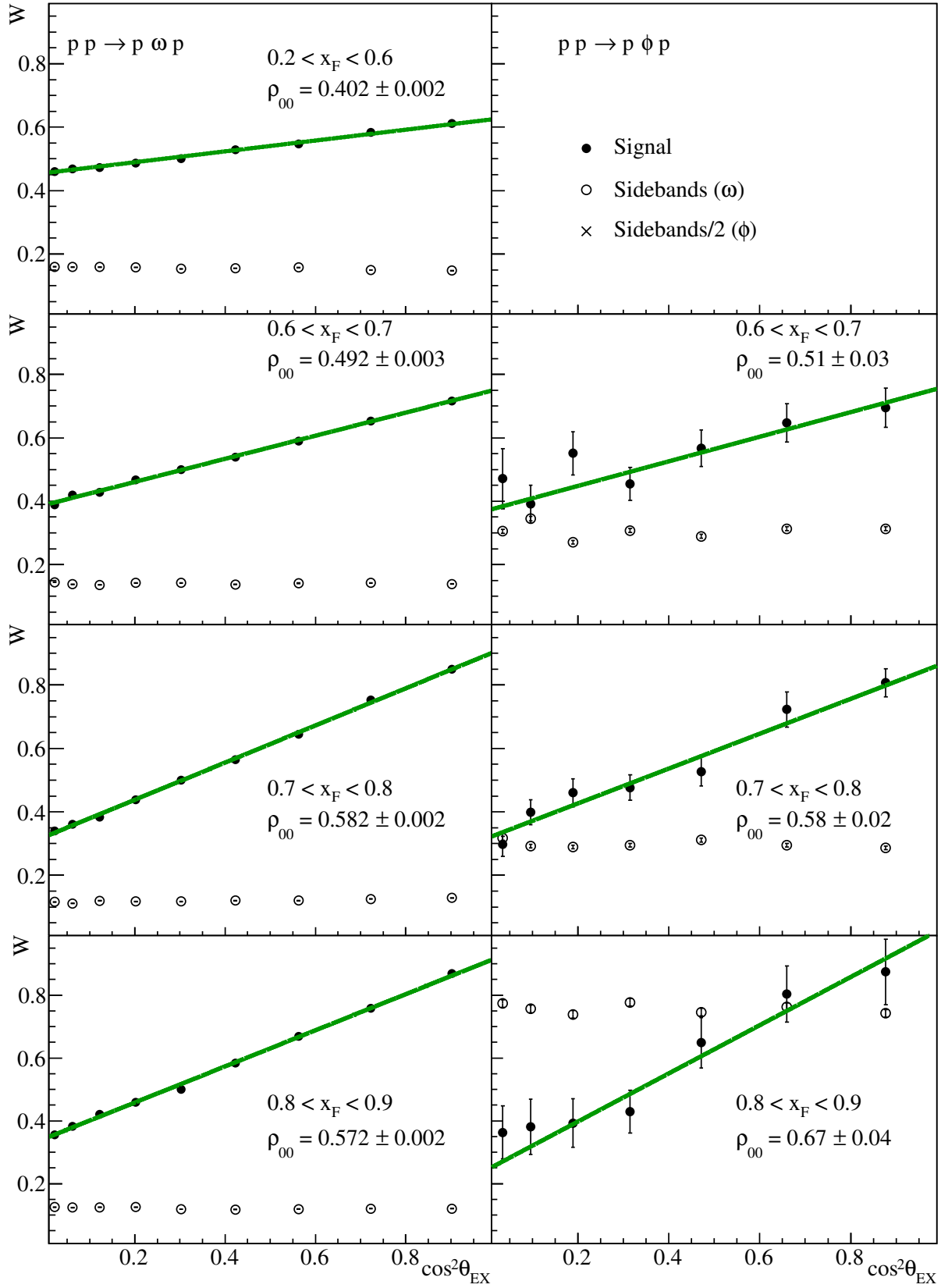


Fig. 12: Angular distributions with respect to $\cos^2 \theta = \cos^2 \theta_{EX}$ using the momentum transfer from p_{beam} to p , $\Delta \vec{P}$, as reference axis. The panels show different x_F regions: 0.2–0.6 (top), 0.6–0.7 (second line), 0.7–0.8 (third line) and 0.8–0.9 (bottom). The error bars include statistical errors and systematics from the background subtraction. The open points show the corresponding distribution for the events in the sidebands around the ω peak in the $M(\pi^+\pi^-\pi^0)$ distribution. The crosses show the corresponding distribution (scaled by 0.5) for the events in the sidebands around the ϕ peak in the $M(K^+K^-)$ distribution. The lines are the results of linear fits as explained in the text.

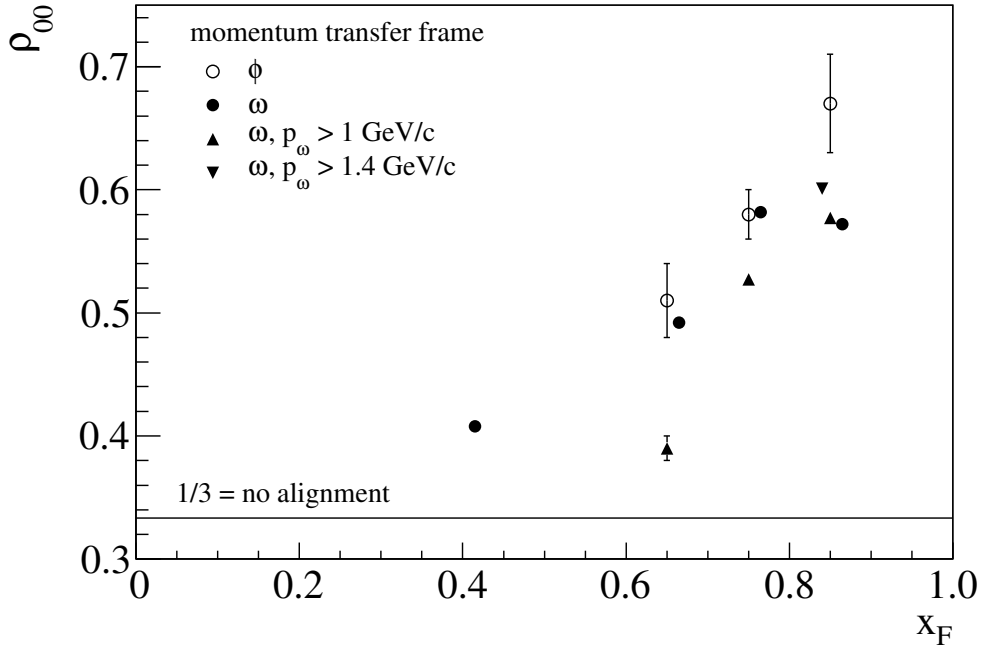


Fig. 13: Spin alignment ρ_{00} extracted using $\Delta\vec{P}$ as reference axis as a function of x_F for different p_V cuts.

angular momentum, then we expect an increasing anisotropy of the vector meson decay in the helicity frame of the N^* with increasing spin of the resonance.

The fact that no structures are visible in the $p\phi$ spectrum and the observation that the ϕ meson is unaligned in the $p\phi$ helicity system indicates that N^* decays into $p\phi$ are OZI suppressed, reflecting the internal structure of the resonance. The observed violation of the OZI rule by a factor of 3-4 (see Table 1) indicates either an admixture of other, OZI-violating reaction processes or a genuine violation of the predicted $g_{\phi NN}^2/g_{\omega NN}^2$ coupling ratio. Note that similar and sometimes smaller values of the OZI violation factor (about 2-3) were observed in Refs. [8, 28–30], all in a kinematic domain where N^* production is prominent.

Removing the low-mass region with visible resonances by a cut on the vector meson momentum in the pV rest system, $p_V > 1.4 \text{ GeV}/c$, *i.e.* $M_{p\omega} > 3.3 \text{ GeV}/c^2$, the picture changes significantly. The ω spin is found to be unaligned with respect to the $p\omega$ system, consistent with the absence of resonances. Furthermore, the OZI violation increases and converges to a factor of about 8, independently of x_F , as can be seen in Table 2. This is in remarkable agreement not only with the SPHINX analysis [8] after removal of the low- $M_{p\omega}$ region, but surprisingly also with data close to threshold from ANKE [31], DISTO [32] and COSY-TOF [33, 34].

The high mass part of the M_{pV} spectrum shows no structures, but may still contain N^* resonances which probably are broad and largely overlap. The angular distributions are isotropic, which means that either low-spin resonances contribute, which is however unlikely in this mass region, or the contribution of resonances is small.

In the high-mass continuum, the decays of ω and ϕ mesons are both strongly aligned with the direction of the 3-momentum transfer $\Delta\vec{P}$. The similar behaviour of the alignments together with larger ρ_{00} values with increasing x_F indicates that the production mechanism is the same for ω and ϕ in this region. This may point to a central Pomeron–Reggeon fusion which produces a vector meson. The OZI violation then reflects a hidden flavour-flow with the emitted Reggeon. The observed x_F dependence of ρ_{00} with respect

to $\Delta\vec{P}$, where ρ_{00} increases with increasing x_F , suggests this process since central production favours large x_F of the fast proton. A different approach to this reaction is obtained assuming an alignment of the spins of the vector meson with the angular momentum of its emission with respect to $\Delta\vec{P}$. Then, the transferred angular momentum has to be perpendicular to $\Delta\vec{P}$. We can regard these events as scattering off a Pomeron radiated from the target proton and absorbed by a colourless object in the beam proton wave function, which carries some fraction of the total momentum. This kind of mechanism may be associated with non-resonant diffractive dissociation. In a very simple picture, the proton dissociates into a proton plus a virtual (off-shell) vector meson V^* (in Ref. [7], this process is referred to as a shake-out). If the Pomeron emitted from the target recoil proton is absorbed by V^* , this could result in an on-shell vector meson recoiling along the direction of momentum transfer of the Pomeron. In other words, we expect that at some energy scale the Pomeron should resolve structures in the extended proton. The data show evidence for this in the observed angular distributions of the vector meson decays, as shown in Figs. 10 and 11 and summarised in Table 5. They exhibit large anisotropies increasing with x_F , which indicates the presence of a transversely localised process with a dependence of its direction on $\Delta\vec{P}$. The high OZI violation indicates a higher effective resolution scale in this process and reflects the probability of finding a preformed ϕ meson relative to the preformed ω meson at a resolution scale near $m_\phi \approx 1 \text{ GeV}/c^2$. The natural angular momentum quantisation axis for such a process is the direction of the momentum transfer mediated by the Pomeron. Both ω and ϕ have substantial alignment of their spins perpendicular to this axis, indicating a transferred orbital angular momentum. The latter is naturally oriented perpendicular to the direction of momentum transfer to which the angular momentum of the vector mesons has a tendency to align if spin-orbit forces occur.

It has been already noted that Pomeron-Pomeron fusion into a $J^{PC}(I^G) = 1^{--}(0^-)$ meson is forbidden due to G -parity conservation. Another theoretical possibility is a central Pomeron-Odderon process¹. Since this process involves no quark lines and the only difference between ω and ϕ is the mass, the ϕ production rate should be of the same order as the ω rate. This is in sharp contrast to our data, in which the ω cross section is thirty times larger than that of the ϕ . Our data therefore show no evidence for Pomeron-Odderon fusion in our kinematic domain ($\sqrt{s}=18.97 \text{ GeV}$, $0.1 < t' < 1.0 (\text{GeV}/c)^2$).

7 Summary and Conclusion

In this work, exclusive ϕ and ω vector meson production in the reaction $pp \rightarrow pVp$ has been measured. We find OZI violations ranging from $F_{\text{OZI}} = 3$ to $F_{\text{OZI}} = 9$ depending on the kinematic region. The invariant mass M_{pV} of the forward proton and the vector meson appears to be the most important kinematic quantity in our study to discriminate processes with different mechanisms. The clear structures in the $M_{p\omega}$ spectrum indicate the importance of $pp \rightarrow pN^*$, $N^* \rightarrow p\omega$ in ω production. This is also supported by the significant alignment of the spin of the ω meson with respect to the direction of the $p\omega$ system. In the case of decays into a ground state vector meson, the N^* has to transfer considerable angular momentum. The absence of structures in the $M_{p\phi}$ spectrum in combination with no observed alignment of the ϕ spin with respect to the direction of the $p\phi$ system shows that the decay of the N^* resonances into $p\phi$ is OZI suppressed. This indicates that the $s\bar{s}$ component of such resonances must be very small. The observed OZI violation by a factor 3-4 in this region could be either due to the admixture of other processes or a genuine violation of the predicted $g_{\phi NN}^2/g_{\omega NN}^2$ ratio.

Removing the resonance region by requiring $M_{p\omega} > 3.3 \text{ GeV}/c^2$, the OZI violation in the remaining kinematic range is significantly higher, typically of order 8 ± 1 . Moreover, the spin of both ω and ϕ are unaligned with respect to the pV system. The behaviour of both vector mesons is the same in the system defined by the transferred momentum. This indicates that the production mechanism in this region for both ω and ϕ is central Reggeon-Pomeron fusion, with the observed OZI violation reflecting a hidden

¹An Odderon is similar to the Pomeron but with negative parity, charge conjugation and G -parity.

flavour flow. This process can also be regarded as a Pomeron resolving preformed colourless objects in the proton wave function and ejecting them in a shake-out. The direction of the transferred momentum is remembered by the vector meson and is manifested in its decay angular distributions. The OZI violation then reflects the probability of resolving a $s\bar{s}$ state in the nucleon.

Acknowledgements

We are grateful to Prof. Colin Wilkin and Prof. Stefan Leupold for helpful discussions. We also gratefully acknowledge the support of the CERN management and staff and the skill and effort of the technicians of our collaborating institutes. Special thanks go to V. Pesaro for his technical support during the installation and the running of this experiment. This work was made possible by the financial support of our funding agencies.

References

- [1] S. Okubo, Phys. Lett. **5** (1963) 165; G. Zweig, Developments in the Quark Theory of Hadrons, Volume 1. Edited by D. Lichtenberg and S. Rosen. pp. 22-101; J. Iizuka, Prog. Theor. Phys. Suppl. **37** (1966) 21.
- [2] H. J. Lipkin, Int. J. Mod. Phys. E **1** (1992) 603.
- [3] H. J. Lipkin, Phys. Lett. B **60** (1976) 371.
- [4] V. P. Nomokonov and M. G. Sapozhnikov, Phys. Part. Nucl. **34** (2003) 94 [Fiz. Elem. Chast. Atom. Yadra **34** (2003) 189] [hep-ph/0204259].
- [5] A. Sibirtsev and W. Cassing, Eur. Phys. J. A **7** (2000) 407 [nucl-th/9907059].
- [6] S. J. Lindenbaum, Nuovo Cim. A **65** (1981) 222.
- [7] J. R. Ellis, M. Karliner, D. E. Kharzeev and M. G. Sapozhnikov, Phys. Lett. B **353** (1995) 319 [hep-ph/9412334]; J. R. Ellis, M. Karliner, D. E. Kharzeev and M. G. Sapozhnikov, Nucl. Phys. A **673** (2000) 256 [hep-ph/9909235].
- [8] S. V. Golovkin, A. P. Kozhevnikov, V. P. Kubarovsky, A. I. Kulyavtsev, V. F. Kurshetsov, L. G. Landsberg, V. V. Molchanov and V. A. Mukhin *et al.*, Z. Phys. A **359** (1997) 435.
- [9] A. Sibirtsev, J. Haidenbauer and U. -G. Meissner, Eur. Phys. J. A **27** (2006) 263 [nucl-th/0512055].
- [10] E. Klempt, F. Bradamante, A. Martin and J. M. Richard, Phys. Rept. **368** (2002) 119.
- [11] K. Gottfried and J. D. Jackson, Nuovo Cim. **33** (1964) 309.
- [12] K. Schilling, P. Seyboth and G. E. Wolf, Nucl. Phys. B **15** (1970) 397 [Erratum:ibid. B **18** (1970) 332].
- [13] F. Bellemann *et al.* [COSY-MOMO Collaboration], Phys. Rev. C **75** (2007) 015204 [nucl-ex/0608047].
- [14] K. Schönning *et al.* [CELSIUS/WASA Collaboration], Phys. Lett. B **668** (2008) 258 [arXiv:0806.2945 [nucl-ex]].
- [15] S. V. Golovkin *et al.* [SPHINX Collaboration], Z. Phys. A **359** (1997) 327.
- [16] M. Abdel-Bary *et al.* [TOF Collaboration], Eur. Phys. J. A **44** (2010) 7 [arXiv:1001.3043 [nucl-ex]].

- [17] C. Daum *et al.* [ACCMOR Collaboration], Nucl. Phys. B **187** (1981) 1.
- [18] B. I. Abelev *et al.* [STAR Collaboration], Phys. Rev. C **77** (2008) 061902 [arXiv:0801.1729 [nucl-ex]].
- [19] J. Barth *et al.* [SAPHIR Collaboration] Eur. Phys. J. A **17** (2003) 269.
- [20] [SAPHIR Collaboration] J. Barth *et al.*, Eur. Phys. J. A **18** (2003) 117.
- [21] A.I. Titov, B. Kämpfer and V.V. Shklyar Phys. Rev. C **59** (1999) 999.
- [22] P. Abbon *et al.* [COMPASS Collaboration], Nucl. Instrum. Meth. A **577** (2007) 455
- [23] GEANT 3.21., CERN program library, Long Writeup **W5013** (1994).
- [24] P. Jasinski, Ph.D. thesis, Mainz University (2011).
- [25] T. Ernst, Diploma thesis, Freiburg University (1985).
- [26] J. Beringer *et al.* [Particle Data Group Collaboration], Phys. Rev. D **86** (2012) 010001.
- [27] S.U. Chung, Spin Formalisms, CERN yellow report CERN-71-8 (1971).
- [28] A. Baldini *et al.*, by H. Schopper, Landolt-Börnstein, New series, Group 1, vol **12**, Springer-Verlag, Berlin (1998).
- [29] R. Baldi *et al.*, Phys. Lett. B **68** (1977) 381.
- [30] V. Blobel *et al.*, Phys. Lett. B **59** (1975) 88.
- [31] M. Hartmann *et al.* [ANKE Collaboration] Phys. Rev. Lett. **96** (2006) 242301
- [32] F. Balestra *et al.* [DISTO Collaboration], Phys. Rev. C **63** (2001) 024004
- [33] S. Abd El-Samad *et al.* [COSY-TOF Collaboration], Phys. Lett. B **522** (2001) 16
- [34] M. Abdel-Bary *et al.* [COSY-TOF Collaboration], Phys. Lett. B **647** (2007) 351